



Space Weather and Solar Wind Studies with OWFA

P. K. MANOHARAN^{1,*}, C. R. SUBRAHMANYA² and J. N. CHENGALUR³

¹Radio Astronomy Centre, NCRA-TIFR, P.O. Box 8, Ooty 643 001, India.

²Raman Research Institute, C. V. Raman Avenue, Sadashivnagar, Bengaluru 560 080, India.

³NCRA-TIFR, Pune University Campus, Ganeshkhind, Pune 411 007, India.

*Corresponding author. E-mail: mano@ncra.tifr.res.in

MS received 21 July 2016; accepted 25 August 2016; **ePublication:** 17 March 2017

Abstract. In this paper, we review the results of interplanetary scintillation (IPS) observations made with the legacy system of the Ooty Radio Telescope (ORT) and compare them with the possibilities opened by the upgraded ORT, the Ooty Wide Field Array (OWFA). The stability and the sensitivity of the legacy system of ORT allowed the regular monitoring of IPS on a grid of large number of radio sources and the results of these studies have been useful to understand the physical processes in the heliosphere and space weather events, such as coronal mass ejections, interaction regions and their propagation effects. In the case of OWFA, its wide bandwidth of 38 MHz, the large field-of-view of $\sim 27^\circ$ and increased sensitivity provide a unique capability for the heliospheric science at 326.5 MHz. IPS observations with the OWFA would allow one to monitor more than 5000 sources per day. This, in turn, will lead to much improved studies of space weather events and solar wind plasma, overcoming the limitations faced with the legacy system. We also highlight some of the specific aspects of the OWFA, potentially relevant for the studies of coronal plasma and its turbulence characteristics.

Keywords. Radio interplanetary scintillation—solar wind—turbulence—space weather events—coronal mass ejections—propagation—disturbances—shock waves.

1. Introduction

One of the successful observational programs being carried out for many years at the Ooty Radio Telescope (ORT) is to determine the three-dimensional structure, evolution and dynamics of quiet and transient solar wind in the Sun–Earth space by using interplanetary scintillation (IPS). These studies have provided valuable inputs to the solar physics community to understand the physical processes in the heliosphere and space weather events, such as coronal mass ejections (CMEs), interaction regions and their propagation effects. These studies have also provided a basis to develop models to predict the effects of such events at 1 AU (e.g., Manoharan 2006; Vršnak *et al.* 2008). However, the present sampling of the heliosphere by the ORT in a day limits the accuracy of such models. It is important to improve on this situation because the practical consequences of space weather demand advance and accurate prediction of space weather effects associated with energetic CMEs. For example, large and high speed Earth-directed CMEs are now considered

to be the major source of transient interplanetary disturbances and shocks, which could cause severe geomagnetic storms and lead to adverse effects on many crucial technological systems (e.g., Kumar *et al.* 2011).

A recent important concern of the solar physics is that a wide array of ground- and space-based observations show that the Sun has entered a sustained period of low activity (e.g., Manoharan 2012; Basu 2016). The current solar cycle #24 seems to be the smallest sunspot cycle observed since cycle #14, which was observed around the beginning of year 1906. The effects of low magnetic activity are observed throughout the heliosphere. Among the prominent effects of this is that the cosmic ray flux near the Earth reached the highest level in the recent past. This in turn leads to various effects in the Earth's atmosphere. The state of the interplanetary medium associated with low solar activity may also influence the effects of propagation of CMEs, formation of shocks, etc., (e.g., Manoharan *et al.* 2016). Thus, an improved global monitoring of the solar wind and transients as well as the space weather conditions at the near-Earth distances would be highly timely.

2. Solar wind measurements

Solar wind observations, to date, have been made mainly in two ways, viz.: (1) directly by *in-situ* sampling of the downstream plasma, (2) remotely, through radio spectroscopy, and radio sounding observations. Since the 1960s a large number of spacecraft have successfully conducted routine *in-situ* sampling of the solar wind (e.g., speed, density, temperature, composition and magnetic field) in the near-Earth space and beyond. However, *in-situ* measurements are limited to the one-dimensional time scan at the location of the spacecraft. Proper measurements of spatial and temporal variations would require a grid of space missions. Moreover, spacecraft sampling is largely confined to the ecliptic plane. Ulysses was the first and only space mission that probed the high latitude heliosphere (e.g., McComas *et al.* 2008).

However, the typical flow of the solar wind and the propagation of solar-generated transients show considerable changes with heliolatitude as well as distance from the Sun. For example, the eruption of a CME/flare event, originating from the complex magnetic region on the Sun, adds significant amount of mass and magnetic field to the solar wind. The propagating transient associated with the CME is about a solar radius in size at the near-Sun region and it can expand to a structure of about an AU in the near-Earth environment (e.g., Manoharan *et al.* 2000). Additionally, CME associated transients can involve: (1) acceleration of electrons and ions to high energies, (2) formation and steepening of interplanetary forward/reverse shocks at distances from the Sun, and (3) propagating/expanding large-scale magnetic clouds (i.e., flux ropes) (e.g., Manoharan 2006; Manoharan & Agalya 2011). Thus, a high occurrence rate of intense flare/CME events can result in the complex flow of solar wind at different time and spatial scales. Therefore, the study of global properties of the solar wind and the efficient tracking of a transient event (as well as in understanding its interaction with the ambient solar wind as a function of distance from the Sun) demand solar wind observations at consecutive parts of the heliosphere and we need to employ techniques and/or observations other than that of *in-situ* measurements from a satellite, which is normally confined to the orbit of the Earth. The radio remote-sensing technique, e.g., interplanetary scintillation, can provide estimates of solar wind speed and density turbulence in the three-dimensional space. However, remote-sensing measurements probe the solar wind plasma integrated along the line-of-sight and hence require care in the interpretation.

2.1 Interplanetary scintillation technique

The IPS technique exploits scattering of radiation from compact radio sources (i.e., radio quasars and galaxies of angular size, $\Theta < 500$ milliarcsecond (mas)) by small-scale (< 1000 km) density inhomogeneities in the solar wind (e.g., Hewish *et al.* 1964; Coles 1978; Manoharan 1993). Since the drift of solar wind density inhomogeneities across the line-of-sight to the source causes intensity scintillation (typically, intensity fluctuations are observed on timescales of ~ 0.1 – 10 s), the shape of the IPS power spectrum is related to the bulk velocity of the density structures and their scale sizes. The power spectrum of intensity fluctuations can be suitably calibrated to estimate the solar wind speed, the level of density turbulence, and the dominant scales present at the region of closest solar approach of the line-of-sight to the radio source (e.g., Manoharan 1993, 2012; Manoharan & Ananthakrishnan 1990; Manoharan *et al.* 2000; Tokumaru *et al.* 1994). Thus, the regular monitoring of the IPS of a given radio source using a single-antenna system of good sensitivity can provide the speed and density turbulence of the solar wind at a range of heliocentric distances (i.e., as the source gradually approaches and recedes the Sun). Additionally, using IPS one can do day-to-day monitoring of the heliosphere on a grid of large number of radio sources, whose lines-of-sight cut across different parts of the heliosphere. The Ooty Radio Telescope is well suited for such monitoring of the inner heliosphere.

2.2 IPS with the Ooty Radio Telescope

The Ooty Radio Telescope (ORT) is an equatorially mounted steerable cylindrical paraboloid (530 m \times 30 m) (Swarup *et al.* 1971), operating at a central frequency of 326.5 MHz. The legacy system of the ORT provides a resolution of $2^\circ \times 6'$, in the East–West and North–South directions, respectively. The ORT covers $-4^{\text{h}}7^{\text{m}}$ to $+5^{\text{h}}25^{\text{m}}$ in hour angle and $\pm 65^\circ$ in declination. The ORT is also supported with a beam-forming system of 12 simultaneous equispaced beams. Each beam is separated by $3'$. For a given declination pointing, this system provides a sky coverage of $36'$ in the North–South direction (Sarma *et al.* 1975; Selvanayagam *et al.* 1993). Over the last several years, IPS observations made with the ORT have been efficiently used to study the dynamics of the interplanetary medium on time scales ranging from a few hours to years.

In the IPS observing mode, since the ORT is fully steerable in the East–West direction, a given

scintillating source can be continuously tracked for $\sim 09^{\text{h}}30^{\text{m}}$ (i.e., from the rise time of the source at the east limit of the ORT to its set time at the west limit) and the solar wind condition along the direction of the source can be monitored in detail. In the above span of observing time, the change in the position of the source with respect to the Sun is not significant (i.e., typically a source moves with respect to the Sun by ~ 1 degree per day) and the continuous tracking observation essentially provides the parameters of the solar wind along a fixed line-of-sight. On the other hand, to scan the solar wind over a wide area of the sky, the ORT can be parked at a convenient hour angle and each source transiting at the telescope can be observed for about 90 s by just electronically switching the North–South beam. A sufficient time gap, if available between the observations of two consecutive sources, can be used to observe the off-source level of IPS, which is required for the estimation of the scintillation index of each observed source (Manoharan 1993; Manoharan *et al.* 1995). In a regular mode of solar wind monitoring, a parking hour angle is chosen close to the east limit of ORT (-4^{h}), which can include the global monitoring of regions, respectively, in the western side of the Sun, close to the Sun, and in the eastern side of the Sun. In such an observing mode, depending on the duration of observation (e.g., 6–8 h), the scintillating sources monitored can cover a wide range of heliolatitudes as well as heliocentric distances in the range of $20\text{--}250R_{\odot}$ in the west as well as east of the Sun and a CME and its associated disturbances propagating in any direction with respect to the Sun can be recorded. Further, the steerability of the ORT allows us to monitor the same part of the sky by parking the ORT, respectively, at hour angles overhead (0^{h}) and near the west limit ($+4^{\text{h}}$) and provides an opportunity to study the temporal and radial evolution of the CME for a period of ~ 20 h (e.g., Manoharan *et al.* 2000, 2001). Alternatively, if an *a priori* information on the propagation direction of a CME is known, the ORT can also be parked at an appropriate hour-angle position and the scintillation of the drifting sources can be studied for a duration of up to ~ 20 h, which can also cover a wide heliocentric distances in the west and east of the Sun.

Moreover, for a given central beam setting of a radio source, the 12-beam system of the ORT often includes one or more sources at other beams away from the central beam and such observations increase the number of sources monitored at a given time. By combining the above hour angle scans, a good spatial resolution in the sky plane is achieved. In the recent past, depending on the other observing programs, the ORT has been used

to make daily observations of about 600–900 radio sources, covering a distance range $\sim 20\text{--}250R_{\odot}$ (corresponding to a solar elongation range of $\sim 5^{\circ}\text{--}100^{\circ}$) in the western and eastern sides of the Sun. The above set of sources monitored normally includes nearly $\sim 90\%$ of scintillators and the remaining are non-scintillators (sources having large angular sizes, $\Theta > 500$ mas). The extended sources are not influenced by the solar wind conditions and are monitored to check the contamination caused by the ionospheric plasma and the level of radio frequency interferences (RFIs), if present. It is to be noted that the ionospheric scintillation, which is rare at 326.5 MHz during the daytime, has different timescales from that of IPS and can also be easily eliminated from the IPS power spectrum.

In the past, a good fraction of the ORT time was used for IPS observations. The regular long-term monitoring of IPS on several radio sources has in fact provided the ‘*scintillation index – heliocentric distance*’ curves of all these sources for several years. Ooty scintillation-index curves are available for ~ 8000 radio sources and these can be used to estimate the typical one-dimensional angular diameter of the compact component of each source as well as its flux density at 326.5 MHz (Manoharan *et al.*, in preparation). Additionally, the scintillation curves obtained from the ORT have been made available to IPS groups at the Solar-Terrestrial Environment Laboratory, Nagoya University, Japan (Tokumaru *et al.* 2011) and the Mexican IPS Radio Array at the University of Mexico, Mexico (González-Esparza *et al.* 2004).

Ooty IPS studies have led to several important results in (1) understanding otherwise unavailable information on the three-dimensional shape and dynamics of the large-scale structures of CME-associated disturbances in the Sun–Earth space (e.g., Manoharan 2010); (2) clearly establishing the speed and associated magnetic structure of CMEs as well as the background solar wind, which are crucial to understand the effects of the CME at the near-Earth environment (Manoharan *et al.* 2001; Manoharan 2006) and these studies have led to the development of propagation models to predict the effects of CME events at ~ 1 AU (e.g., Mays *et al.* 2015); (3) the relationship between the speed and transit time of CME-associated disturbances; (4) the three-dimensional evolution of density turbulence and speed of quasi-stationary solar wind at various levels of solar activity over a period of three decades (e.g., Manoharan 1993, 2012); (5) a better understanding of the nature of turbulence and plasma processes of the ambient solar wind in the inner heliosphere and the solar wind plasma associated with the interplanetary

disturbance (e.g., shape of the density turbulence spectrum and its dissipative scales as the function of distance from the Sun) (Manoharan *et al.* 1987, 1994, 2000).

2.3 IPS imaging with the legacy ORT system

Figure 1(a) shows example of a scintillation image obtained with the ORT based on observations of about 600 IPS sources on 16 January 2015. These observations were taken over a time period of ~ 18 h at an hour-angle pointing of 0^{h} and nearly equal regions were sampled in the western and eastern hemispheres of the heliosphere. This plot is the sky-plane snapshot image of level of density turbulence in solar wind, observed over a heliocentric distance range of more than an AU from the Sun. (For more details on the Ooty IPS analysis and the construction of scintillation image, the reader may refer to Manoharan *et al.* 2001.) The image area is made of 600×600 pixels (i.e., covering a heliosphere diameter of about 3 AU). Since the image is made from scintillation observations of a large number of discrete radio sources, it has been smoothed by a two-dimensional Gaussian of width 20×20 pixels. The radius of the concentric circles drawn around the Sun increases in steps of $50R_{\odot}$. The orbit of the Earth is located at $\sim 215R_{\odot}$. The observing time increases from the right of the image (the west of the Sun) to the left (the east of the Sun). The red color code indicates the background (i.e., ambient) solar wind. The enhanced scintillation regions represent the CME-driven disturbances and/or interactions between slow and fast solar wind streams. For example, the propagation of two CMEs that originated from the Sun on 13 and 15 January 2015 are seen in the north-east direction of the Sun, respectively, at $\sim 225R_{\odot}$ and $100R_{\odot}$. Apart from these, some more faint enhanced features are also identifiable in Fig. 1(a).

As mentioned above, this scintillation image has been made from IPS observations of ~ 600 radio sources and the distribution of these sources around the Sun is shown in Fig. 1(b). Each dot in the plot corresponds to a radio source. The noted asymmetry in the source distribution between the north and south regions of the heliosphere is due to the allowed declination coverage of $\pm 60^{\circ}$ for the above IPS measurements (i.e., at high declinations $> |\pm 45^{\circ}|$, the sensitivity of the ORT is severely affected by the decrease in the projected collecting area). The radio sources employed are of flux density ≥ 1 Jy at 326.5 MHz. It may be noted that the overall source distribution is not uniform and

there are several small to large gaps seen in the plot. In particular, at heliocentric distances $> 150R_{\odot}$ the number of sources observed is less than that observed at small distances from the Sun. This is mainly due to the fact that the radial falloff of the power of density turbulence in the solar wind is rather steep, $C_{N_e}^2(R) \sim R^{-4}$, and the scintillation of a source would also decrease with the distance from the Sun in the above manner. At 326.5 MHz, for a point source (e.g., $\Theta \leq 20$ mas), the maximum level of scintillation is observed at $\sim 40R_{\odot}$ and it is reduced by an order of magnitude at $\sim 150R_{\odot}$ (Manoharan *et al.* 1995). In the present legacy system of the ORT, we employ a receiver system bandwidth of ~ 4 MHz centered around 326.5 MHz and use an integration time on each source of ~ 90 s. This enables the detection of a scintillation flux of ~ 25 mJy. In the legacy system, for a given observing period, the number of sources observed is therefore limited by their compact component flux densities as well as angular sizes. However, the Gaussian smoothing function used to smooth an image area of $\sim 20 \times 20$ pixels enables the detection of overall large-scale structures of the three-dimensional solar wind. Further, CMEs in general propagate with high speed (i.e., speed in excess of the background solar wind speed of $\sim 300\text{--}350$ km s $^{-1}$) and the present spatial resolution provided by the distribution of sources is just enough to sample the propagating CME structures at a couple of places in the inner heliosphere (e.g., Manoharan *et al.* 2001). Thus, IPS observations with the present legacy system have limited the detailed inference of the small-scale features of solar wind, CMEs and interaction regions. Another important point is that the temporal cadence obtained for a fast moving CME in a day is low and hence precise study of such fast moving CMEs is difficult with the present IPS measurements alone.

3. IPS with the Ooty Wide Field Array (OWFA)

In order to improve the study of fine features of CMEs, solar wind structures and to predict their arrival times and associated consequences at the near-Earth space about a day in advance, the essential requirement is the imaging of the interplanetary medium with further increased spatial and temporal resolutions. In comparison with the legacy ORT system, the upgraded OWFA has both a large instantaneous bandwidth of ~ 38 MHz and a significantly wide North–South beam of $\sim 27^{\circ}$ (refer to Subrahmanya *et al.* 2017). For example, at a given time, the large declination coverage of the OWFA beam would allow the simultaneous observation of a

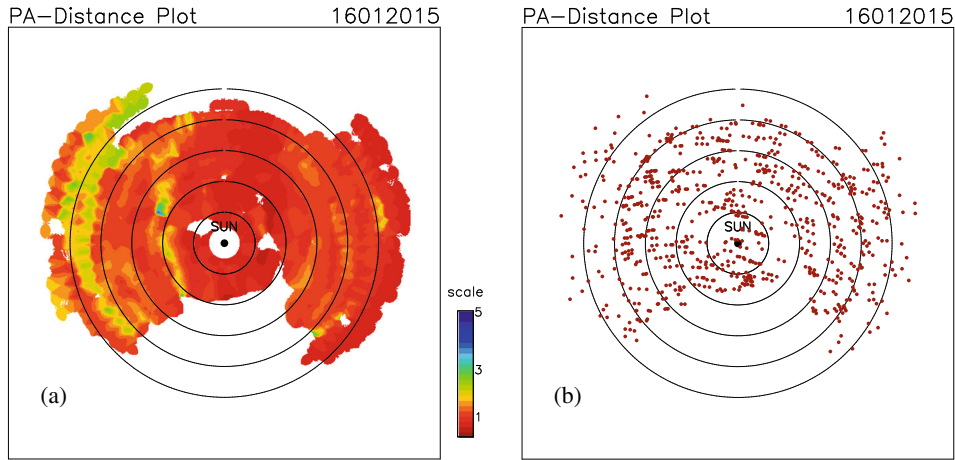


Figure 1. (a) An example of scintillation image observed with the ORT on 16 January 2015. It shows the sky-plane projection of observed levels of density turbulence in the solar wind in the inner heliosphere and the Sun is at the centre of the image. The red color code indicates the background solar wind and the enhanced scintillation patches indicate the presence of interplanetary CMEs in the IPS field-of-view. (b) A similar plot is the distribution of IPS sources observed to make the scintillation image and each dot represents the position of a radio source. The plotted IPS field-of-view includes ~ 600 radio sources. In these ‘position angle (PA) – heliocentric distance’ plots, the north is at the top, i.e. PA = 0° and PAs 90° , 180° and 270° , respectively, correspond to the east, south and west of the Sun. Observing time increases from the right-hand side of the plot (i.e., from the west of the Sun) to the left-hand side (i.e., the east of the Sun). The concentric circles are of radii 50, 100, 150, 200 and $250R_\odot$.

number of IPS sources covered within its beam. Additionally, the increase in the sensitivity of the OWFA by a factor ~ 3 would enable the observation of sources with weak scintillating flux density.

The OWFA will have an FX correlator with a bandwidth of ~ 38 MHz and with 800 spectral channels (Subrahmanya *et al.* 2017; Subrahmanya & Chengalur, in preparation). Phased array beam formation will be done post-correlation. Since the OWFA baselines are highly redundant (with only 264 of the 34716 baselines being unique), the post correlation beam formation can be done very efficiently. The visibility on the each of the unique baselines can be estimated by averaging over the multiple redundant copies. The data volume is now so drastically reduced that one can form simultaneous phased array beams covering the entire field-of-view corresponding to the primary beam of the individual OWFA elements. All sources of interest lying within the primary beam can hence be simultaneously monitored. This real-time beam forming requires high cadence, real-time calibration of the antenna gains, for which fast redundancy calibration algorithms have been developed and tested for OWFA (Marthi & Chengalur 2014).

For the parameters of the OWFA system, a simulated source distribution (for observations on 15 September 2016) is shown in Fig. 2(a). The source lists used for making the above simulation include (1) the

existing list of IPS scintillators obtained from the ORT long-term monitoring, which includes sources of flux density ≥ 1 Jy at 326.5 MHz, and (2) sources of flux density ≥ 0.7 Jy at 326.5 MHz, scaled from the Texas and Molonglo surveys, respectively, made at 365 and 408 MHz (Douglas *et al.* 1996; Large *et al.* 1981). This simulation has been done for an hour-angle pointing of $\sim 0^h$ and an observing time span of ~ 18 h, centered around the transit time of the Sun on 15 September 2016 and it is generated for an observing situation similar to that presented in Fig. 1. The OWFA beam has been scanned from -65° to $+65^\circ$ in a step of $\sim 20^\circ$, which allows considerable overlap between one beam setting to the other. In a beam setting, all the sources of flux density ≥ 0.7 Jy contained in the primary beam area of $2^\circ \times 27^\circ$ are considered. However, if more than one source is located within the beam size of the full ORT, $2^\circ \times 6'$, it is counted as a single source. The number of sources included in the simulated distribution is more than 5500, which is about an order of magnitude larger than the number of sources observed with the legacy system (refer to Fig. 1). In comparison with the legacy system, the above source distribution obtained for the OWFA nearly fills the imaged area and large gaps are almost absent. Since the improved sensitivity of the OWFA allows the observation of sources with small scintillating flux density, the simulated coverage looks nearly uniform throughout the 3-AU heliosphere.

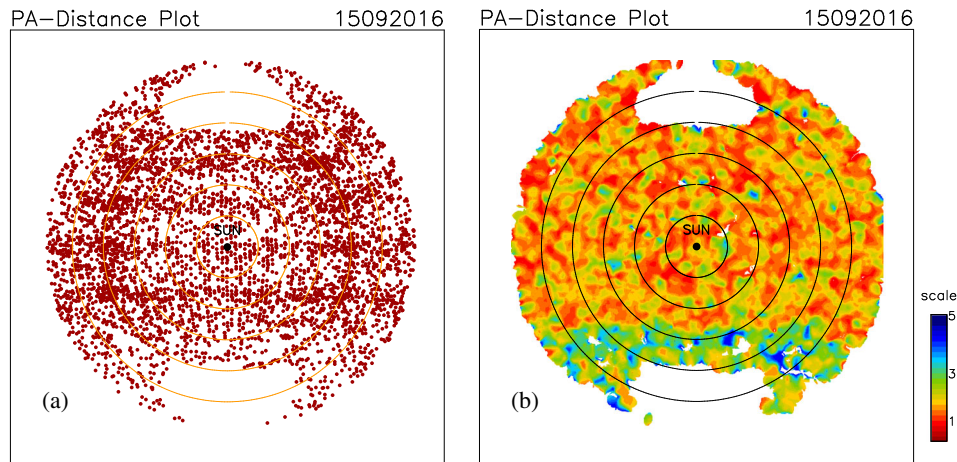


Figure 2. (a) A simulated source distribution possible with the OWFA for an IPS monitoring on 15 September 2016. It includes ~ 5500 radio sources and each dot on the plot corresponds to a radio source. (b) The simulated scintillation image obtained for the above source distribution. These plots are similar to Fig. 1.

It is to be noted that the above simulation includes only sources of $S_{326.5} \geq 0.7$ Jy. But, since IPS is not much limited by the confusion limit of the system, the OWFA can therefore observe sources weaker than the above limit. Since the number density of the source increases with decreasing flux density, the IPS with the OWFA is expected to provide more finer spatial resolution than that discussed above.

Figure 2(b) shows the typical two-dimensional image obtained from the above simulated source distribution. In order to make this image, a uniform level of 50% of the source flux density is taken as the level of scintillation and the maximum allowed scintillation is limited at 5 units. It is equivalent to Fig. 1(a) and covers an area of 600×600 pixels. The simulated image has been smoothed by a two-dimensional Gaussian of width 5×5 pixels, which is 16 times smaller than the area used in smoothing the image obtained with the legacy system (refer to Fig. 1). It is evident that the image is not smooth and shows number of fine features. Such an image on a short observing time span will provide information on small-scale structures embedded within a CME as well as their evolution characteristics. The quick scanning of the OWFA beam would also allow to image the fast moving CMEs and study their dynamics with the IPS measurements alone.

IPS observations of small flux density sources aimed with the OWFA are also likely to lead to the detection of ultra compact radio sources possibly at high red shift. The increase in sensitivity of the OWFA by a factor of ~ 3 not only enables the observation of small flux density sources, but will also provide an excess of ~ 5 dB signal in the estimated power spectrum (Naidu *et al.* 2015). This will be useful to infer the characteristics of small dissipative scales (i.e., at scales < 25 km,

Manoharan *et al.* 1994, 2000, 1987) of the density turbulence. These studies are crucial to understand the evolution of density turbulence and the behaviour of the dissipative scales in the solar wind, which, in turn are essential to understand the physical processes associated with the solar wind plasma. The turbulence spectrum can also be studied as functions of (1) distance from the Sun, (2) heliographic latitude or source region of solar eruption, and (3) solar activity phase.

3.1 Reconstruction of heliosphere

Since the IPS with the legacy system provides observations on a grid of large number of sources per day, it allows the reconstruction of the three-dimensional heliosphere using the time-dependent computer-assisted tomography technique (CAT) developed at the University of California, San Diego (Manoharan 2010; Jackson *et al.* 2003). The basic data sets required for the three-dimensional reconstruction are the time series of solar wind speed and level of scintillation for a large number of lines-of-sight of the heliosphere. Even with the limited number of lines-of-sight, the reconstructions made with the legacy system of the ORT have given several important results (Bisi *et al.* 2009; Manoharan 2010). The much better coverage of the OWFA would hence provide an improved understanding of the dynamical heliosphere.

3.2 IPS picket fencing with the OWFA

In order to probe fine structure in a CME, the legacy ORT system was employed in a couple of special type

of IPS observations, in which only a few IPS sources (i.e., only two or three lines-of-sight) were selected such that they lie at the expected crossing location of the radially moving CME and its associated interplanetary disturbance. The continuous monitoring of a few radio sources at frequent interval (about 2 min on each line-of-sight) allows one to estimate (1) ambient solar wind before the arrival of the CME at the IPS lines-of-sight; (2) the properties of plasma along the radial cut through the shock, sheath and CME; (3) the upstream flow behind the interplanetary disturbance (Manoharan 2010).

Even though IPS measurements are integrated along a line of sight, they are still useful to study the characteristics of the plasma within the CME and the solar wind moving ahead and behind the disturbance. The CME study using this ‘picket-fence’ method with the OWFA will allow observations of large number of lines-of-sight for a given distance from the Sun. For example, in Fig. 2(a), if we consider a circular ring of constant radius running from the north pole to south pole of the inner heliosphere, several sources will lie on the circular ring. The simple beam switching between these sources would provide high cadence sampling, at times before, during a CME passage, and after its crossing. Such set of observations at two or more radial distances can give detailed information on (1) internal structure of the CME and its variations as a function of radial distance, (2) overall size of the CME and its evolution with distance, (3) the shock forming location in front of the CME, (4) stand-off distance/time (i.e., distance or time between the driver gas and the shock), and (5) dynamics of the shock and sheath. Such studies can also be useful to infer the particle acceleration site as well as the effective acceleration encountered by the CME in the solar wind (Manoharan 2006). They are also vital to understand the energy of the solar wind as well as the energy transfer between the disturbance and the surrounding ambient medium.

As in the picket-fence method, if we examine the circular rings of varying radii at the polar regions above the Sun, it can provide new information on the fine structure of polar plumes, their temporal evolution and relationship with other transient phenomena. Polar plumes are thin long ray kind of structures observed above the polar coronal holes and they can extend up to a distance of several solar radii. The OWFA would help to observe the polar solar wind on much finer spatial and temporal scales, allowing the study of plasma processes associated with the polar plumes. In a similar way, OWFA IPS program will also help to investigate the plasma associated with coronal jets

above the limb of the Sun. Such studies could be essential in understanding the plasma processes linked to the coronal heating problem.

4. Summary

In this paper, we briefly discuss the ongoing IPS observing program with the legacy system of the ORT and its limitations in understanding the details of physical processes associated with CMEs and the solar wind in the Sun–Earth distance range. The upgraded ORT, the OWFA, will have a large field-of-view and improved sensitivity and allow observations of about an order of magnitude large number of IPS sources. Thus, its unique ability to sample large areas of the interplanetary medium with unprecedented spatial and temporal resolutions gives the OWFA advantages over all current radio telescopes. The OWFA can be potentially useful in addressing, but not limited to, the following studies: (1) it can enhance the inference of dynamics of space weather events, in particular, fast moving CMEs and improve the predictability of their arrival at the near-Earth space; (2) the tomographic reconstruction of IPS with OWFA is expected to provide a clear view of the global heliosphere; (3) detailed IPS studies on limited number of radio sources can be useful to probe different parts of a CME, its associated shock, sheath, and their influence on the surrounding ambient solar wind; (4) the capability of OWFA also allows to select a given region of the heliosphere and investigate its plasma characteristics.

Acknowledgements

The authors thank the observing/engineering team of Radio Astronomy Centre for the help in forming the critical component of this project. They thank A. Johri for helpful conversation and reading of the manuscript. This project is partially supported by the Indian Space Research Organisation (ISRO sanction order no. E.33011/35/2011-V).

References

- Basu, S. 2016, *Living Reviews in Solar Physics*, **13**(2), doi: [10.1007/s41116-016-0003-4](https://doi.org/10.1007/s41116-016-0003-4).
- Bisi, M. M., Jackson, B. V., Clover, J. M., Manoharan, P. K., Tokumaru, M., Hick, P. P., Buffington, A. 2009, *Ann. Geophys.*, **27**, 4479–4489, doi: [10.5194/angeo-27-4479-2009](https://doi.org/10.5194/angeo-27-4479-2009).

- Coles, W. A. 1978, *Space Science Reviews*, **21**, 411–425, doi: [10.1007/BF00173067](https://doi.org/10.1007/BF00173067).
- Douglas, J. N., Bash, F. N., Bozyan, F. A., Torrence, G. W., Wolfe, C. 1996, *Astronomical Journal*, **111**, 1945, doi: [10.1086/117932](https://doi.org/10.1086/117932).
- González-Esparza, J. A., Carrillo, A., Andrade, E., Pérez-Enríquez, R., Kurtz, S. 2004, The MEXART interplanetary scintillation array in Mexico, in: *Geofis. Int.*, p. 61.
- Hewish, A., Scott, P. F., Wills, D. 1964, *Nature*, **203**, 1214–1217, doi: [10.1038/2031214a0](https://doi.org/10.1038/2031214a0).
- Jackson, B. V., Hick, P. P., Buffington, A., Kojima, M., Tokumaru, M., Fujiki, K., Ohmi, T., Yamashita, M. 2003, Time-dependent tomography of hemispheric features using interplanetary scintillation (IPS) remote-sensing observations, *Solar Wind Ten*, edited by M. Velli, R. Bruno, F. Malara and B. Bucci, volume 679 of American Institute of Physics Conference Series, pp. 75–78, doi: [10.1063/1.1618545](https://doi.org/10.1063/1.1618545).
- Kumar, P., Manoharan, P. K., Uddin, W. 2011, *Solar Physics*, **271**, 149–167, doi: [10.1007/s11207-011-9805-7](https://doi.org/10.1007/s11207-011-9805-7).
- Large, M. I., Mills, B. Y., Little, A. G., Crawford, D. F., Sutton, J. M. 1981, *MNRAS*, **194**, 693, doi: [10.1093/mnras/194.3.693](https://doi.org/10.1093/mnras/194.3.693).
- Manoharan, P. K. 1993, *Solar Physics*, **148**, 153–167, doi: [10.1007/BF00675541](https://doi.org/10.1007/BF00675541).
- Manoharan, P. K. 2006, *Solar Physics*, **235**, 345–368, doi: [10.1007/s11207-006-0100-y](https://doi.org/10.1007/s11207-006-0100-y).
- Manoharan, P. K. 2010, *Solar Physics*, **265**, 137–157, doi: [10.1007/s11207-010-9593-5](https://doi.org/10.1007/s11207-010-9593-5).
- Manoharan, P. K. 2012, *ApJ*, **751**(2), 128.
- Manoharan, P. K., Agalya, G. 2011, *Advances in Geosciences, Volume 27: Solar Terrestrial (ST)*, **27**, 165–179.
- Manoharan, P. K., Ananthakrishnan, S. 1990, *MNRAS*, **244**, 691–695.
- Manoharan, P. K., Ananthakrishnan, S., Dryer, M., Detman, T. R., Leinbach, H., Kojima, M., Watanabe, T., Kahn, J. 1995, *Solar Physics*, **156**, 377–393, doi: [10.1007/BF00670233](https://doi.org/10.1007/BF00670233).
- Manoharan, P. K., Ananthakrishnan, S., Pramesh Rao, A. 1987, IPS observations of solar wind in the distance range 40–200 R_{sun} , in: *Sixth International Solar Wind Conference*, edited by V. J. Pizzo, T. Holzer and D. G. Sime pp. 55–57.
- Manoharan, P. K., Kojima, M., Gopalswamy, N., Kondo, T., Smith, Z. 2000, *ApJ*, **530**, 1061–1070, doi: [10.1086/308378](https://doi.org/10.1086/308378).
- Manoharan, P. K., Kojima, M., Misawa, H. 1994, *Journal of Geophysical Research*, **99**, 23411–23420, doi: [10.1029/94JA01955](https://doi.org/10.1029/94JA01955).
- Manoharan, P. K., Maia, D., Johri, A., Induja, M. S. 2016, Interplanetary consequences of coronal mass ejection events occurred during 18–25 June 2015, in: *Coimbra Solar Physics Meeting: Ground-based Solar Observations in the Space Instrumentation Era*, volume 504 of Astronomical Society of the Pacific Conference Series, edited by I. Dorotovic, C. E. Fischer and M. Temmer, pp. 59–66.
- Manoharan, P. K., Tokumaru, M., Pick, M., Subramanian, P., Ipavich, F. M., Schenk, K., Kaiser, M. L., Lepping, R. P., Vourlidas, A. 2001, *ApJ*, **559**, 1180–1189, doi: [10.1086/322332](https://doi.org/10.1086/322332).
- Marthi, V. R., Chengalur, J. 2014, *MNRAS*, **437**, 524–531, doi: [10.1093/mnras/stt1902](https://doi.org/10.1093/mnras/stt1902).
- Mays, M. L., Taktakishvili, A., Pulkkinen, A., MacNeice, P. J., Rastätter, L., Odstrcil, D., Jian, L. K., Richardson, I. G., LaSota, J. A., Zheng, Y., Kuznetsova, M. M. 2015, *Solar Physics*, **290**, 1775–1814, doi: [10.1007/s11207-015-0692-1](https://doi.org/10.1007/s11207-015-0692-1).
- McComas, D. J., Ebert, R. W., Elliott, H. A., Goldstein, B. E., Gosling, J. T., Schwadron, N. A., Skoug, R. M. 2008, *Geophysical Research Letters*, **35**(18), L18103, doi: [10.1029/2008GL034896](https://doi.org/10.1029/2008GL034896).
- Naidu, A., Joshi, B. C., Manoharan, P. K., Krishnakumar, M. A. 2015, *Experimental Astronomy*, **39**, 319–341, doi: [10.1007/s10686-015-9450-5](https://doi.org/10.1007/s10686-015-9450-5).
- Sarma, N. V. G., Joshi, M. N., Bagri, D. S., Ananthakrishnan, S. 1975, *IETE Journal of Research*, **21**(3), 110–116, doi: [10.1080/03772063.1975.11450642](https://doi.org/10.1080/03772063.1975.11450642).
- Selvanayagam, A. J., Praveenkumar, A., Nandagopal, D., Veluswamy, T. 1993, *IETE Technical Review*, **10**, 333–339.
- Subrahmanya, C. R., Prasad, P., Girish, B. S., Somashekar, R., Manoharan, P. K., Mittal, A. K. 2017, *J. Astrophys. Astr.*, doi: [10.1007/s12036-017-9434-0](https://doi.org/10.1007/s12036-017-9434-0) (this issue).
- Swarup, G., Sarma, N. V. G., Joshi, M. N., Kapahi, V. K., Bagri, D. S., Damle, S. H., Ananthakrishnan, S., Balasubramanian, V., Bhave, S. S., Sinha, R. P. 1971, *Nature Physical Science*, **230**, 185–188, doi: [10.1038/physci230185a0](https://doi.org/10.1038/physci230185a0).
- Tokumaru, M., Kojima, M., Fujiki, K., Maruyama, K., Maruyama, Y., Ito, H., Iju, T. 2011, *Radio Science*, **46**(5), RS0F02, doi: [10.1029/2011RS004694](https://doi.org/10.1029/2011RS004694).
- Tokumaru, M., Kondo, T., Mori, H., Tanaka, T. 1994, *Journal of Geomagnetism and Geoelectricity*, **46**(10), 835–849.
- Vršnak, B., Vrbanec, D., Calogović, J. 2008, *Astronomy and Astrophysics*, **490**, 811–815, doi: [10.1051/0004-6361/200810215](https://doi.org/10.1051/0004-6361/200810215).